Theoretical and Applied Climatology
https://doi.org/10.1007/s00704-018-2737-5

ORIGINAL PAPER

Analysis of spatial and temporal variability of aerosol optical depth over China using MODIS combined Dark Target and Deep Blue product

Mikalai Filonchyk[1,2] · Haowen Yan[1,2] · Zhongrong Zhang[3]

Received: 18 May 2018 / Accepted: 29 November 2018

Abstract

This study reviews spatial and temporal variability of aerosol optical depth (AOD) at 550 nm, obtained with Moderate Resolution Imaging Spectroradiometer (MODIS) (Terra) Collection 6.1 aerosol products with use of combined Dark Target and Deep Blue algorithm. Data was analyzed for 18-year period from 2000 to 2017 over the territory of the whole continental China, covering the largest cities as well as various ecological and geographical regions. Spatial distribution of AOD has distinct geographical differences with gradual decrease from the east to the west of the country. The lowest values (up to 0.25) of annual mean AOD at 550 nm occur in sparsely populated areas on the Tibetan Plateau and in the north forest ecosystems in the north-eastern part of China. Areas of desert and semidesert landscapes of Northwest China are characterized by high concentrations of naturally occurring aerosols with moderate values of AOD (0.4–0.7). The most populous regions (Pearl River Delta, Yangtze River Delta, North China Plain, and Sichuan Basin) with the highest density of agricultural and industrial activity are characterized with maximum values of AOD (over 0.7). Seasonal variation of aerosols in the most regions of China has maximum AODs in spring or summer and minimum in autumn or winter. Ångström exponent (AE), being 0.31–1.7 for the most part of China, was used to detect the size of aerosol particles, with the lowest values (0.31–0.84) in desert north and north-west regions of the country, and the higher values in the south (1.3–1.7). Comparison of results, obtained with MODIS Terra and AERONET (Aerosol Robotic Network) at 550 nm, demonstrate a high interrelation ($r = 0.8949$), where 68.3% fall within the range of expected errors, set by MODIS over the land ($\pm 0.05 \pm 0.15 \times \mathrm{AOD}$). The conducted Pearson's correlation analysis between various cities of the country showed that cities in one region with shortest distances from one another demonstrated higher correlations, suggesting distinct regional dependence in aerosols distribution.

1 Introduction

Relevance of atmospheric aerosols investigations is conditioned by the fact that at the surface layer aerosol particles are atmospheric air pollutants, and at a global scale it is one of key factors, affecting climate (Kang et al. 2015; Georgeson et al. 2016). The essential factor of environmental and man-induced changes in global climate is atmospheric aerosol. It is associated with its impact on transfer both short-wave and long-wave radiation and, consequently, on the underlying surface radiation balance (Bian et al. 2009), atmosphere, and Earth's surface-atmosphere system (Sellers 1969), as well as on all dynamic, physical, and chemical processes in atmosphere (Seinfeld and Pandis 1998). At the same time, aerosol particles, accumulating a number of chemical substances, turn into one of principal atmospheric pollutant (Xia et al. 2013; Hu et al. 2014) and affect public health (Thurston et al. 2015; Watts et al. 2015) and economic activity (Huang et al. 2016). World Health Organization (WHO) recommendations offer to set severe restrictions on particulate matter concentration in atmospheric air. Since national network of air quality monitoring may provide only locate data for aerosols for a restricted region due to unavailability or rareness of monitoring stations in the most districts of the country, the use of remote satellite sounding enables to define substances

✉ Haowen Yan
haowen2010@gmail.com

Mikalai Filonchyk
filonchyk.mikalai@gmail.com

[1] Faculty of Geomatics, Lanzhou Jiaotong University, Lanzhou 730070, China

[2] Gansu Provincial Engineering Laboratory for National Geographic State Monitoring, Lanzhou 730070, China

[3] School of Mathematics and Physics, Lanzhou Jiaotong University, Lanzhou 730070, China

Published online: 18 December 2018

concentrations in atmosphere with high spatial and temporal resolution with use of aerosol optical depth (AOD) (Hong et al. 2010; Deng et al. 2013; Kang et al. 2016).

As known, atmospheric aerosol has a significant impact on the atmospheric state for two reasons: first, the direct effect due to solar radiation absorption and distribution; second, indirect effects on weather processes manifested in the fact that aerosol particles act as water vapor condensation center, thus influencing the cloud formation process. The cloud cover, in its turn, determines the visible and IR radiation absorption and distribution by the atmosphere and characterizes the Earth's albedo (Penner et al. 2001).

AOD is one of basic optical parameters and a key parameter for evaluation of aerosol content in atmosphere and air pollution level, is a key factor in determination of aerosol radiation effects sensing (Dickerson et al. 1997; Kim et al. 2004; Sayer et al. 2015). For example, the AOD can be measured to assess aerosol load on the atmosphere (Xia et al. 2007, 2008; Li et al. 2010; Che et al. 2015a, 2015b). AOD spectral dependence expressed by the Ångström parameter, as well as the study of the relationship between Ångström parameter and AOD can be useful for identifying aerosol types (Xin et al. 2007). The aerosol particles content in the air column may be estimated by measuring, in several spectral channel at the top atmospheric border, the infrared radiation brightness going away from the Earth. Moderate Resolution Imaging Spectroradiometer (MODIS) data make it possible to estimate the atmospheric AOD describing the full content of particulate matters in the atmospheric column (Ichoku et al. 2002; Kaufman et al. 2005; He et al. 2012a, 2012b; Qi et al. 2013).

In recent years, the large number of satellite data used to characterize the worldwide aerosols distribution widely apply MODIS data. Many research groups offered various algorithms for aerosols monitoring with use of MODIS. Thus, some researchers have made their efforts to verify the algorithms for aerosols search, their gradual modernization and improvement (Zhang and Reid 2010; Levy et al. 2007, 2010, 2013). For instance, Kaufman et al. (1997) offered Dark Target (DT) approach, which later was modified by Levy et al. (2013). This approach provides for receiving aerosol data over an ocean and vegetation cover and over other dark earth areas. However, due to high surface reflecting capacity, this approach failed against bright reflecting surfaces (Remer et al. 2005). For this reason, use of Dark Target algorithm over desert environment is impossible as it leaves large spatial gaps in AOD values. However, Hsu et al. (2004, 2006, 2013) proposed a brand new Deep Blue (DB) algorithm, which enables to use relatively low reflection rate of desert and other surfaces in deep blue ranges to obtain aerosol properties. That is why Deep Blue algorithm was developed to obtain data on aerosols over deserts and other arid surfaces, and later on it was enhanced to cover earth surface with vegetation (Lee et al. 2016).

Although a lot of studies, aimed at research of aerosol products from MODIS satellite as well as Aerosol Robotic Network (AERONET) ground-based stations, were carried out in China, however, the majority of these studies were restricted by particular cities or regions (Li et al. 2012; Xin et al. 2014; You et al. 2015; Filonchyk et al. 2018a). Some of studies were focused on research of AOD characteristics over different types of surfaces, such as various orographic units, including both plain (Xia et al. 2013) and elevated (Xia et al. 2008), mountain (Li et al. 2011), and desert territories (Che et al. 2013; Ge et al. 2015; Zong et al. 2015), as well as urbanized to different degree city (Xia et al. 2007; Che et al. 2015a) and rural areas (Wang et al. 2013), cities in major rivers basins (He et al. 2010; Song et al. 2014). Other studies were focused on research of various sets of data from MODIS Collection 6 and 5.11 (Li et al. 2007; Leeuw et al. 2018), as well as interrelations between MODIS aerosol products and similar products from other sensors (e.g., MISR and SeaWiFS) (Shi et al. 2011; Cui et al. 2012; Qi et al. 2013; Kang et al. 2016). Nevertheless, the most part of data about aerosol products is given for several large cities or East China (Bilal and Nichol 2015). As it is difficult to establish comprehensive AOD climatology over China due to a very little number of studies, aimed at research of MODIS aerosol product in the area of the entire continental China, and restriction of AOD temporal data, used in the aforementioned studies, it was decided to conduct this study with use of several sets.

Taking into account swift economical and social development of the country, China experienced sharp increase of industrial and agricultural activity and, consequentially, increase of energy consumption, accompanied by significant anthropogenic aerosols emissions in the atmosphere. For this reason, depending on origin, aerosols over the territory of China are referred to various types, including dust, sulfate, and carbonic. Thus, in order to consolidate the understanding of aerosols impact on climatic change as well as their evolution, it is critical to analyze long-term trends and variability in AOD over China for the last decades. This article reviews spatial and temporal variability of annual and seasonal average values of AOD in different regions of the country, covering the entire territory of continental China based on 18-year long-term data as well as investigation of relationship between AERONET ground-based stations and data, received from MODIS Terra satellite with use of combined Dark Target, Deep Blue AOD at 550 nm for land and ocean aerosol products during the period from 2000 to 2017.

2 Data and methodology

This study covers the territory of the entire country and was conducted in 31 large cities, situated in the territory of continental China, which simultaneously serve as province capitals and cities of central subordination (Beijing (BJ), Shanghai (SH) Chongqing (CQ), and Tianjin (TJ)). Geographical map of China, shown in Fig. 1, is traditionally divided into six geographical areas, designated by different solid colors. Regions used in this study are as follows: North China (BJ and TJ; Hebei, Inner Mongolia, and Shanxi provinces), Northeast China (Jilin, Heilongjiang, and Liaoning provinces), East China (SH; Zhejiang, Jiangsu, Fujian, Jiangxi, Shandong, and Anhui provinces), South Central China (Hubei, Henan, Hunan, Guangxi, Guangdong, and Hainan provinces), Southwest China (CQ; Sichuan, Guizhou, Yunnan, and Tibet provinces), and Northwest China (Qinghai, Gansu, Shaanxi, Xinjiang, and Ningxia provinces). Table 1 presents in detail information on aerosol monitoring sites. This study enables to understand spatial and temporal variability of AOD from MODIS.

To analyze spatial and temporal distribution of aerosol in the atmosphere over the territory of China, we used data from MODIS satellite sensor, which is the Imaging Spectroradiometer, mounted on NASA satellites Terra (launched on December 18, 1999). Satellites move along polar orbit with inclination 98.5°, with period 99 min and height 705 km, cross the Line from north to south at about 10:30 a.m. and from south to north around 1:30 a.m. local time. Data on AOD in spectral channel MODIS 550 nm was used to investigate aerosols dynamics and optic properties. Spatial resolution of radiometer at this wave length was 1 × 1° for investigation of large areas and with spatial resolution 3 km for investigation aerosols within urban agglomerations. Areas of altitudes, studied by Spectroradiometer, cover altitudes from tropopause (9–12 km) to surface atmosphere. Radiometer MODIS enables to perform daily on-line monitoring of areas with periodicity of observations depending on their sizes and geographical location as well as number of satellites used. Due to a broad field of MODIS vision (2330 km on the earth surface), periodicity of observation of a separate area with shooting by one satellite is one to two times in day time and the same at night. With shooting by two satellites, the monitoring frequency increases from 4 to 12 times a day (depending on geographical location of the area).

MODIS instrument on board of Terra satellite provides high-quality measurement and extraction of aerosols properties for more than 15 years (Platnick et al. 2003, 2017). The previous version of MODIS data, known as Collection 6, replaced the outdated Collection 5.1. This Collection included updates of both calibration methodology and algorithms of aerosols search (Levy et al. 2013; Platnick et al. 2017). One of the essential updates in Collection 6 was inclusion of combined data set of Dark Target and Deep Blue algorithms (Levy et al. 2013). However, starting from summer 2017, MODIS Adaptive Processing System (MODAPS) began to generate the improved Collection 6.1 for all products of MODIS Level-1/2/3 atmosphere level. This decision on creation of a new improved Collection 6.1 was conditioned by the need to address a number of problems in the current collections 6 Level-1B (L1B). These problems in L1B to different extent affected the lower level products MODIS Atmosphere Level-2 (L2)

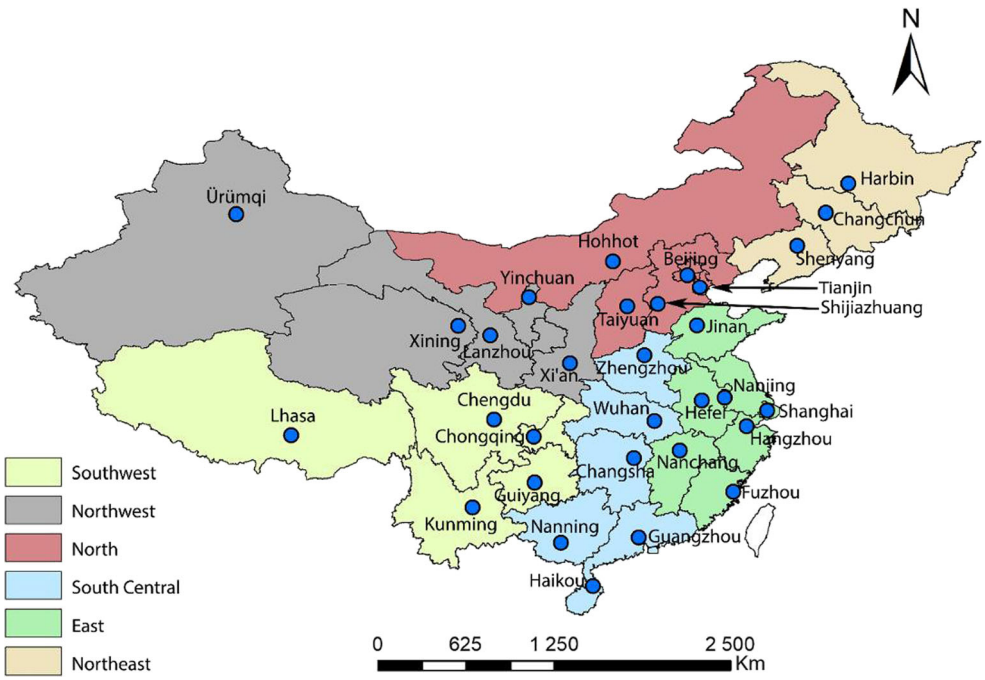

Fig. 1 Geographical locations of the study regions

Table 1 Geographical information about regions of study in China

Region	Area (km^2)	Population(million)	Provinces and region	Provincial and regional seat	Latitude and longitude
North China	1,556,061	164.82	Beijing	Beijing (BJ)	N39°56′ E116°24′
			Tianjin	Tianjin (TJ)	N39°08′ E117°11′
			Hebei	Shijiazhuang (SJZ)	N38°04′ E114°29′
			Shanxi	Taiyuan (TY)	N37°52′ E112°33′
			Inner Mongolia	Hohhot (HH)	N40°49′ E111°39′
Northeast China	793,300	109.52	Liaoning	Shenyang (SY)	N41°47′ E123°26′
			Jilin	Changchun (CC)	N43°54′ E125°12′
			Heilongjiang	Harbin (HB)	N45°45′ E126°38′
East China	795,837	384.36	Shanghai	Shanghai (SH)	N31°13′ E121°28′
			Jiangsu	Nanjing (NJ)	N32°03′ E118°46′
			Zhejiang	Hangzhou (HZ)	N30°15′ E120°10′
			Anhui	Hefei (HF)	N31°52′ E117°17′
			Fujian	Fuzhou (FZ)	N26°04′ E119°18′
			Jiangxi	Nanchang (NC)	N28°41′ E115°53′
			Shandong	Jinan (JN)	N36°40′ E116°59′
South Central China	1,014,354	383.55	Henan	Zhengzhou (ZZ)	N34°46′ E113°39′
			Hubei	Wuhan (WH)	N30°35′ E114°17′
			Hunan	Changsha (CS)	N28°11′ E112°58′
			Guangdong	Guangzhou (GZ)	N23°08′ E113°16′
			Guangxi	Nanning (NN)	N22°49′ E108°19′
			Hainan	Haikou (HK)	N20°02′ E110°20′
Southwest China	2,365,900	192.98	Chongqing	Chongqing (CQ)	N29°33′ E106°34′
			Sichuan	Chengdu (CD)	N30°39′ E104°03′
			Guizhou	Guiyang (GY)	N26°39′ E106°38′
			Yunnan	Kunming (KM)	N25°04′ E102°41′
			Tibet	Lhasa (LS)	N29°39′ E91°07′
Northwest China	3,107,701	96.65	Shaanxi	Xi'an (XA)	N34°16′ E108°54′
			Gansu	Lanzhou (LZ)	N36°02′ E103°48′
			Qinghai	Xining (XN)	N36°38′ E101°46′
			Ningxia	Yinchuan (YC)	N38°28′ E106°16′
			Xinjiang	Ürümqi (UQ)	N43°49′ E87°36′

and Level-3 (L3). For these reasons, it was necessary to use this processing potential to implement some improvements in the area of perfection of L2 and L3 products. That is why the new issue of MODIS was rid of material inconsistencies and potential search problems, identified in the past. Inclusion of combined Dark Target and Deep Blue of aerosol product in Collection 6, and later in Collection 6.1, was reasoned by decision to provide more complete information on filling gaps in data sets, which were received using algorithms apart from one another with changes in the products themselves. The expected extraction accuracy evaluation of Deep Blue and Dark Target AOD ranges within $\pm 0.05 \pm 0.20 \times$ AOD (Hsu et al. 2013; Sayer et al. 2014, 2015) and $\pm 0.05 \pm 0.15 \times$ AOD (Levy et al. 2013) over the land. For this reason, this study uses data from new Collection 6.1 for MODIS Atmosphere Level-3 and Level-2 products based on daily and monthly mean combined Dark Target, Deep Blue AOD at 550 nm for land and ocean (MOD08_M3, MOD08_D3, and MOD04_3K). Taking into account that both satellites were launched and started to be used at different times, this study uses data from satellite MODIS Terra from February 2000 to December 2017 with use of Scientific Data Set named "AOD_550_Dark_Target_Deep_Blue_Combined."

3 Results and discussion

3.1 Interannual variation and trends in aerosol optical depth

Aerosol component is the essential and permanent element, present at the Earth's lower atmosphere, which is responsible

not only for passing of optical part of spectrum through atmospheric depth, but serves as absorbent of thermal part of energy, coming from the Sun to the Earth. One of the criteria, characterizing attenuation of optical emission in the environment due to absorption and scatter, is optical depth. In other words, AOD is optical property of aerosol column, which describes the degree of aerosols scatter or absorption, which will decrease solar irradiation before it reaches the Earth's surface.

Average monthly AOD values at wavelength 550 nm, obtained with MODIS Terra spectroradiometer with spatial resolution 1°, were used as source information. Figure 2 shows mean annual and seasonal AOD values for the period from 2000 to 2017 for the entire territory of China. In this regard, an analysis of long-term linear trends based on averaged (average daily values) across the country annual mean and seasonal mean AOD values was carried out. Generally, annual average temporal series of AOD showed a trend to decline from 0.392 in 2000 to 0.267 in 2017 with gradual decrease by 0.125, with trends of − 0.01. Note that in spring, when considering trends of AOD changes, reduction from 0.420 in 2000 to 0.331 in 2017 with decrease by 0.089, with trends of − 0.008 for the whole territory of the country is observed. Summer AOD values during 18-year monitoring demonstrate sinusoidal form with distinct peaks in 2003 (0.449), 2007 (0.424), 2011 (0.451), and 2014 (0.416) with gradual reduction of values from 0.449 in 2007 to 0.292 in 2017 with decrease of value by 0.157 and with trends of − 0.013. In autumn, as in the case with other seasons, a tendency to gradual reduction, however, not so obvious as in other seasons is observed with change from 0.231 in 2000 to 0.209 in 2017 with decrease of value by 0.022 and trend for 18-year period − 0.002 (confidence level 99%). Based on average daily mean values for seasonal and annual change of AOD with sampling of 6449 days, correlation analysis (r) was carried out, which showed negative correlation between AOD values and seasons with standard errors (SE) of deviation from trend with annual mean values 0.0024, suggesting slight degree of deviation. Standard uncertainty was used to study the effect of MODIS uncertainties on the analysis of trends in AOD, which was the uncertainty of the measurement result expressed as standard deviation (SD) equal to 0.145. The smallest values of uncertainty were in the autumn (SD = 0.085) and winter (SD = 0.091) periods, low uncertainty indicated the prevalence of the local sources of pollution. However, the increasing influence of uncertainty manifests itself in the spring (SD = 0.153) and summer (SD = 0.123) periods demonstrated that, in addition to local sources, there were natural aerosols, which were transported from the desert regions of the country and had an impact throughout the country. Also, the meteorological parameters in the summer period contributed to the formation of aerosols and at the same time to the increase in uncertainties in this period. At the same time, a small negative trend could be associated with uncertainty obtained in the AOD or instrument calibration (Levy et al. 2010).

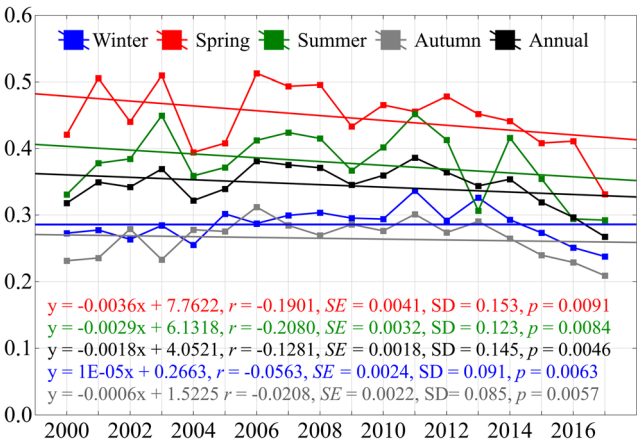

Fig. 2 Annual and seasonal AOD time series averaged for the period 2000–2017 for China, together with the slopes, correlation coefficient (r), standard error (SE), standard deviation (SD), and p value (p) of the linear trends

3.2 The spatial distribution of aerosol optical depth and Ångström exponent over China

Pattern of spatial variability of mean values of AOD in the territory under analysis is illustrated in Fig. 3. Areas in figures, designated with white background, represent absence of data on AOD monitoring. Figure 3 shows spatial distribution of MODIS Terra AOD at 550 nm over China, suggesting that aerosols significantly affect many regions of the country. One of the reasons for this territory selection to conduct study is that the whole territory of China with large urban, suburban, industrial, coastal, mountainous, and desert regions is very diverse, resulting in various weather conditions, which, in its turn, impacts aerosols loading in each region of the country. As is seen from Fig. 3, mean decennial AOD value in the east of China is significantly higher, than in the west, suggesting serious geographical differences in aerosols loading levels. Clear relationship between population density in the country regions and aerosols concentration is observed. It is related to the fact that the East and South China as well as the metropolitan region with over 70% of the country population (Table 1) are characterized with large urban and industrial agglomerations with large amount of emissions, resulting from industrial, agricultural, and domestic needs. It suggests that these circumstances are likely to be responsible for high levels of AOD in these regions.

The spatial pattern of AOD distribution over China is characterized by several centers of high, moderate, and low AOD values. High AOD values (over 0.7) are registered over the territory of North China Plain and the East China (Hebei, Shanxi, Shandong, Anhui, and Jiangsu provinces), Central China (central and eastern part of Hubei and north of Hunan provinces) as well as Sichuan Basin (eastern part of Sichuan

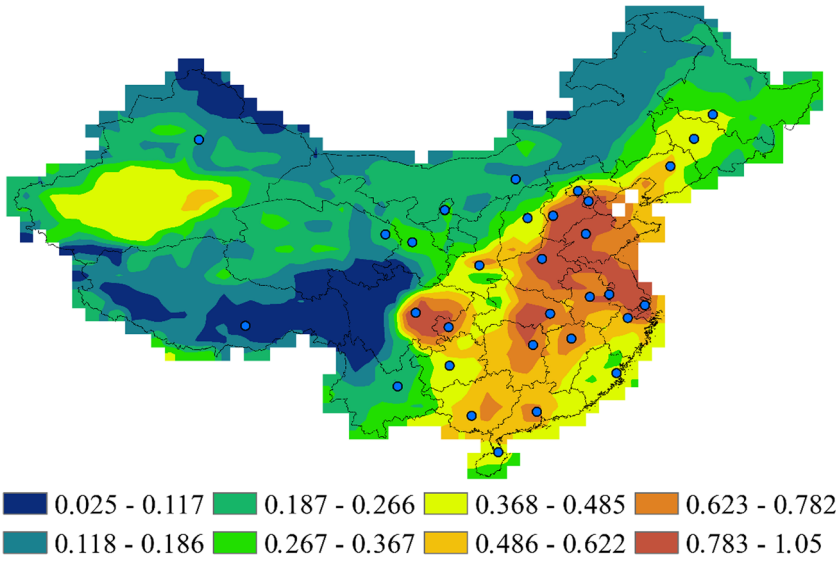

Fig. 3 Spatial distribution of 18-year averaged AOD (550 nm) over China retrieved from MODIS Terra products for the period 2000–2017

Province and CQ). This is due to the fact that this area houses the most densely populated and industrialized regions with low elevation and high anthropogenic aerosols emissions (North and East China). In these regions with the highest AOD values, a great amount of finely dispersed aerosols are accounted for by the sources from anthropogenic activity and characterized by local emissions of anthropogenic aerosols, resulting in great aerosols loading of the territory (Zhao et al. 2013; Huang et al. 2018; Che et al. 2015b).

Moderate AOD values (0.4–0.7) were in North East (central and south part of the region), Northwest (Tarim Basin), Southeast, and South China. High AOD values, which were in Tarim Basin in the southern part of Xinjiang, were characterized by high concentrations of naturally occurring aerosols, in which desert dust, emitted from the Taklamakan Desert, might predominate (Xia et al. 2008).

Regions with the lowest AOD values (up to 0.25) were in the north, north-west (Qinghai), and south-west (Tibet, Yunnan, and west of Sichuan Province) parts of China. As these districts are scantily populated and restricted in emissions of industrial aerosols, aerosols loadings in these regions remain low throughout the year. Besides, very low AOD values were observed in regions of dense natural forest vegetation cover in high-latitude Inner Mongolia and Heilongjiang regions of the country.

Eighteen-year statistics of mean annual AOD values over the territory of China showed in Fig. 3, according to which multi-year mean AOD value of 0.38 occurred in the period of 2000 to 2017. Average data on AOD over the territory of China show clear spatial differences and are changed from the east to the west of the country. Thus, maximal values are registered in the territory of North China Plain (0.741–1.009) and Sichuan Basin (0.707–0.944), South Central China (0.616–0.725), Tarim Basin (from 0.374 to 0.542), Northeast China (0.336–0.603) to North China (0.138–0.342) and Tibet (0.05–0.223).

In order to evaluate the accuracy of MODIS Terra Collection 6.1 Dark Target and Deep Blue merged aerosol product, a dependence of MODIS Terra against AERONET AOD at 550 nm wavelength was carried out. We interpolate the sun photometer AOD values at 440 and 675 to 550 nm, to provide a common wavelength for both satellites and AERONET. The error of AOD observations from automatic solar photometers of the global AERONET network in the visible region of the solar spectrum does not exceed 0.01 (at a wavelength longer than 440 nm) (Holben et al. 1998), and the observations of these photometers are taken as standart. In general, the quality of aerosol search by the MODIS spectrometer depends on the accuracy of the surface reflectivity and the aerosol model, and overestimation and understatement of results on clear and polluted days are usually caused by the error of these factors. Based on data, received from 14 AERONET stations, located in different regions of China, analysis of accuracy evaluation with data, received from MODIS Terra with spatial resolution 3 km (MOD04_3K product) over AERONET stations in the relevant days of investigation, was carried out. Pairs of MODIS AOD and AERONET data were considered aggregated, if time difference between the two obtained samples did not exceed 30 min with spatial resolution $0.3 \times 0.3°$. The study uses the AERONET AOD Level 2 data for the period 2001–2017. Figure 4 shows that out of 7159 pairs of sampling 68.3% (4889 pairs) search results are within the expected error (EE) and demonstrate a high relationship ($r = 0.8949$) with $SE = 0.0045$ and $SD = 0.256$ with a high degree of reliability (confidence level 99%). Thus, the chosen algorithm may be used for quantitative studies of aerosols and their application in various regions.

Ångström exponent (AE), being the characteristics parameter of AOD dependence on wave length and indicating the size of aerosol particles, was used to study the size of particles,

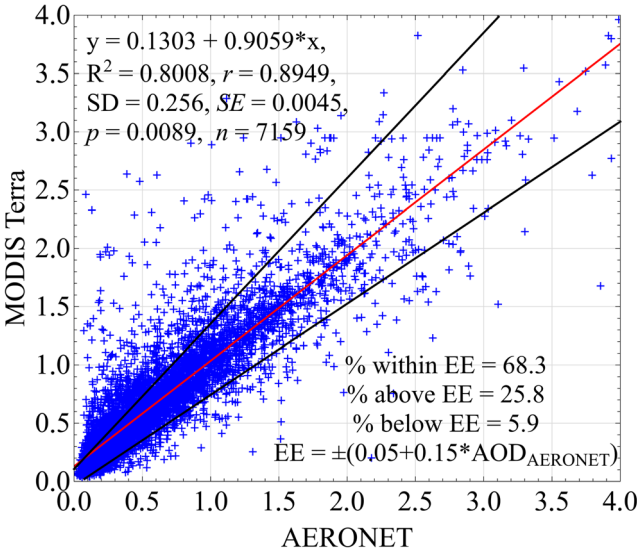

Fig. 4 Scatterplots between the Collection 6.1 of MODIS Dark Target and Deep Blue merged AOD at 550 nm against the corresponding AERONET retrievals for the 14 sites (AOE_Baotou (E109° 629′ N40°852′), Beijing (E116°381′ N39°997′), Dunhuang_LZU (E94°955′ N40°492′), Hangzhou-ZFU (E119°727′ N30°257′), Hefei (E117°162′ N31°905′), Lanzhou_City (E103°853′ N36°048′), Zhongshan_Univ (E113°390′ N23°060′), XiangHe (E116°962′ N39°754′), Zhangye (E100°276′ N39°079′), Taihu (E120°215′ N31°421′), SACOL (E104°17′ N35°946′), City_GZ (E113°158′ N23°081′), Jingtai (E104°1′ N37°333′), Minqin (E102°959′ N38°607′)). (The red line is the regression line, and the black lines define the envelope of EE)

present in atmosphere. In the present study, the values of AE are computed in the wavelength interval 440–870 nm. In general, AE range from 0.0 to 2.0, whereas lesser AE values correspond to the larger size of aerosol particles (Kim et al. 2004). Figure 5 shows spatial AE variability, distributed over China, received from MODIS Terra sensor for the period from 2000 to 2017. It is apparent from the figure that AE ranges from 0.31 to 1.8 for the most part of the country with the lower values between 0.31 and 0.84 in the north and north-west of the country, and the higher values—in the south (1.3–1.8). According to Fig. 5, one of the main sources of coarse particles formation as a result of wind erosion is the Taklamakan Desert. It was also found that AE has not associate with AOD in the majority of China regions. This indicates that increase of AOD over the North China Plain occurs predominantly with those aerosols with a large size of dust particles, which are transported from deserts of North and Northwest China and Republic of Mongolia (Luo et al. 2013; Kang et al. 2015). Moreover, dust blown by wind and generated by construction works, vehicles, branches of industry, favorable weather conditions, and poor vegetation cover in this region also contributed to the high AOD observed (Qiu et al. 2016).

The least AE values were found along the east and south coastal regions of the country, where sea-salt aerosols from South China, East China, and Yellow Seas prevail, as well as in the north and south-west parts of China, characterizing by a great amount of desert dust particles, transported from the Taklamakan Desert as well as deserts which are part of the Gobi Desert. It suggests that dust from the Earth surface is the essential source of local coarse particles. In addition, terrain orography and human activity also significantly impact AE distribution. It is difficult for coarse particles to reach more upland earth areas by way of vertical exchange in the atmospheric boundary layer (Filonchyk et al. 2016; Ye et al. 2018). Thus, thick vegetation, mountainous areas with low density of population and deficit of human activity as well as restriction of coarse particles due to orography contribute to high AE values and consequently low AOD values. Anthropogenic activity generates a great amount of finely dispersed aerosol particles in densely populated urban and industrial districts, resulting in AOD increase. Nevertheless, in addition to more

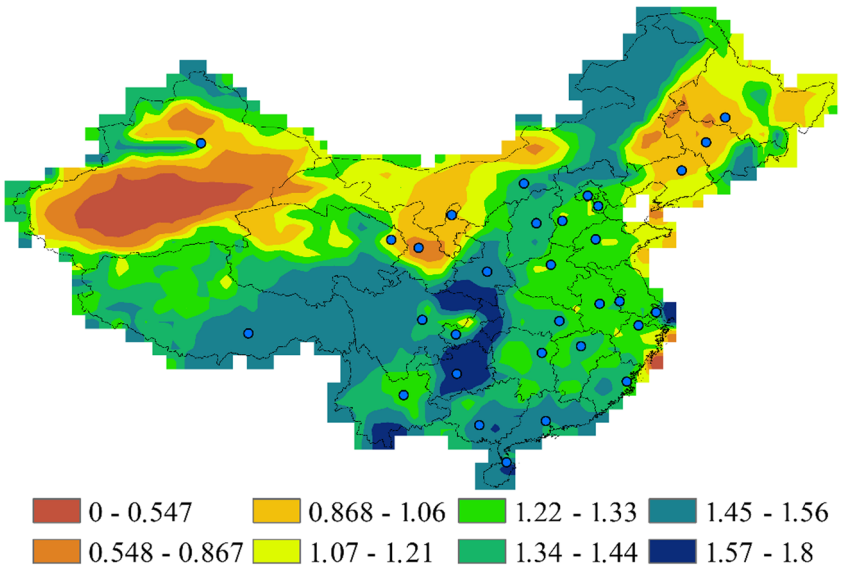

Fig. 5 Spatial distribution of 18-year averaged Ångström exponent (440/870 nm) over China retrieved from MODIS Terra products for the period 2007–2017

coarse particles of soot from industrial and civil consumption of fossil fuel (Gerelmaa et al. 2016), air dust, resulting from motor vehicles exhausts and construction works in urban areas, causes formation of coarse particles, which command a large part in the total content of aerosol particles in the atmosphere, resulting in lower AE values in urban areas, than in suburban and mountainous.

Diagram of AOD distribution compared to AE is shown in Fig. 6. As seen, there is a trend to AOD increase with decreasing AE, which means large particles presence in the atmosphere. Local or regional dust events are the most likely source of this type of aerosols. There are also cases when AOD and AE values are about 0.5 and 1.0, respectively, which probably reflects the presence of small particles, such as black carbon and sulfate (Che et al. 2013). In general case, the interlink between AOD and AE can be well described based on linear regression equation, $y = 1.3607 - 0.607x$ where $R^2 = 0.2983$.

3.3 Seasonal and monthly mean MODIS Terra AOD distributions over the territory of China

Aerosols emission from natural and anthropogenic sources alters in these sources from time to time. Besides, some meteorological conditions influence on AOD distribution, such as humidity and temperature (affect on secondary particles formation), precipitations (affect on particle settling), and wind (affect on particles transport and dispersion). In order to understand temporal variability of aerosol, monthly and seasonal AOD characteristics were analyzed in China.

Based on data on Fig. 7, during the entire period of observations over the whole territory of China, a seasonal cycle of AOD dynamics was observed, suggesting strong aerosol seasonality in all regions of the country. Spatial distribution of seasonal average AOD was identical to spatial structure of multiannual average AOD. Winter, spring, summer, and autumn AOD distribution in the entire territory of continental China in the period 2000–2017 is shown in Fig. 7. Seasonal AOD distribution is characterized by high and low centers of AOD values, which remain practically unchanged during four seasons. Seasonal average AOD values over China varied in the order spring→summer→winter→autumn, with maximum in spring (0.466), summer (0.379), winter (0.360) to minimum in autumn (0.277). This seasonal pattern suggests that spring may be the most polluted season in the entire territory of China, probably due to maximal loading of dust aerosols, transported from deserts of North and Southwest China, as well as due to high levels of biomass combustion and flying dust from natural surfaces in spring period. One of the reasons of high AOD values in summer is higher air temperatures, which tend to hold atmospheric water vapor, increasing atmospheric aerosols capacity for hygroscopic growth (Xu et al. 2006; Li et al. 2007). Other sources of fine particles in aerosol, such as grassland and forest fires as well as biomass combustion, have certain temporal regularities and are typically occurring in the harvest season from June to August. During crop harvesting, a great amount of straw is combusted, generating heavy smoke for the ambient air, and this significantly increases optical depth (Luo et al. 2001). Note that in the period 2000–2017 in all regions of the country high concentrations in winter were likely produced due to increase of emissions, caused by coal combustion in that season.

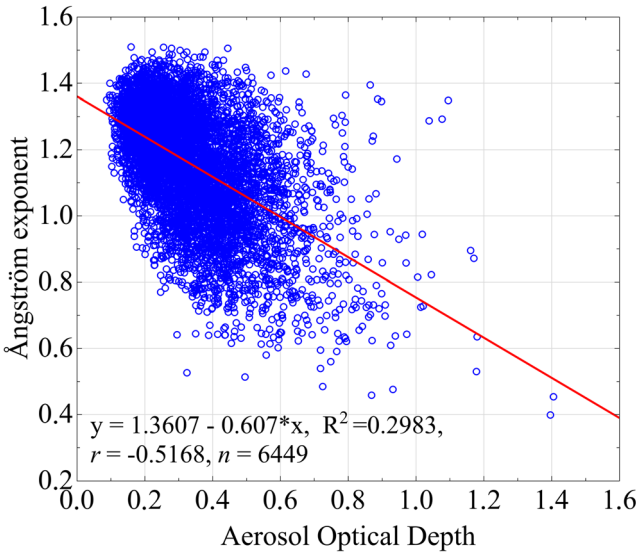

Fig. 6 Relationship between AOD and AE

Depending on seasonal variations of aerosol sources, significant AOD variability from season to season was observed in regions with high AOD values, such as Northwest, East China as well as metropolitan region and Sichuan Basin. Anthropogenic aerosol emissions in these regions are associated with seasonal cycle of human activity, including agriculture, transport, and industry. Dust storms, which result in formation of natural dust aerosols in Northwest China, are more frequent in spring (Filonchyk et al. 2018a, 2018b), so transportation of dust aerosol during dust storms in spring may also increase aerosol loading in this region and contribute to aerosol distribution into other adjacent regions of the country. Relatively low AOD variability in all seasons was similar to annual mean values over Southwest China at the intersection of Tibet, Sichuan, and Qinghai provinces and characterized by minimal AOD values against other regions of the country. This may be associated with low density of population, which leads to minimal business activity at these areas.

3.4 Temporal variability of AOD over various ecological regions of China

Temporal series, such as monthly variability in various ecological regions of China, were formed based on monthly mean

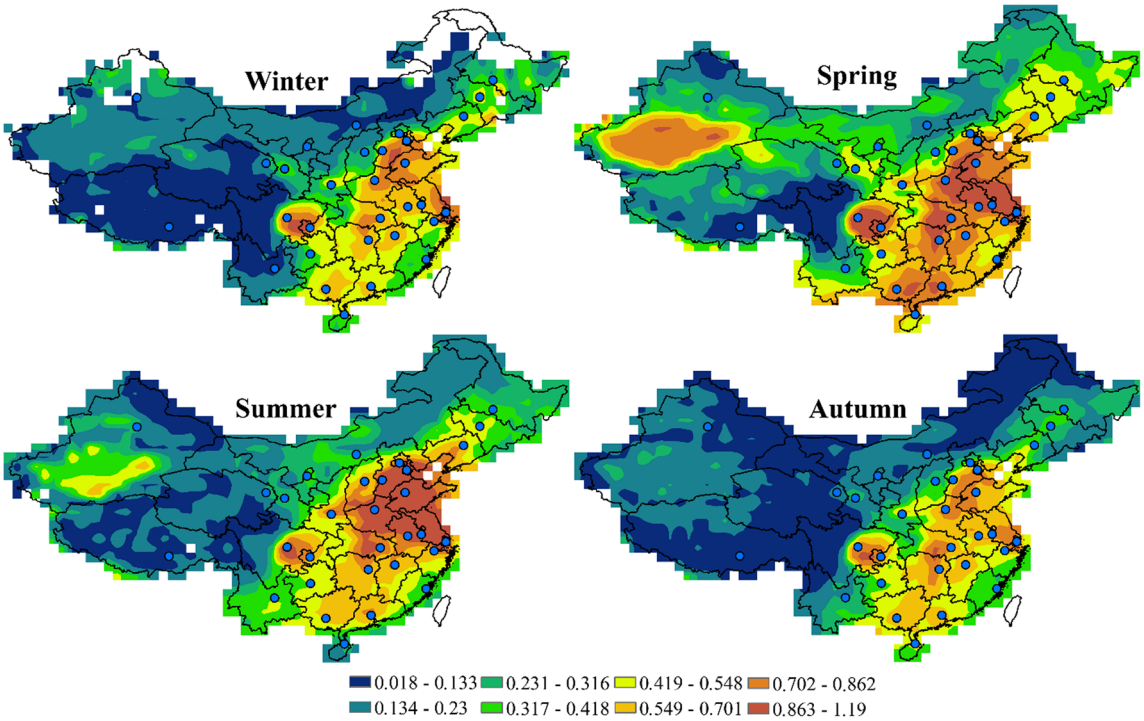

Fig. 7 Seasonal mean AOD over China for the period 2000–2017

values of AOD for 18 years. Figure 8 presents monthly variability of AOD in regions, which to different extent is exposed to AOD. Because of the fact that the eastern part of China in general is more exposed to anthropogenic activity, and the western part—to the impact of natural sources (Li et al. 2012; Che et al. 2013; Guan et al. 2015; Filonchyk et al. 2016), such as dust storm, eight typical China regions were distinguished. These regions were selected to the intent that they cover different ecological regions with complicated and diverse relief, with various climatic conditions, with desert and forest landscapes, coastal districts and hinterlands, with densely populated and underpopulated territories, which to different extent are exposed to natural and anthropogenic

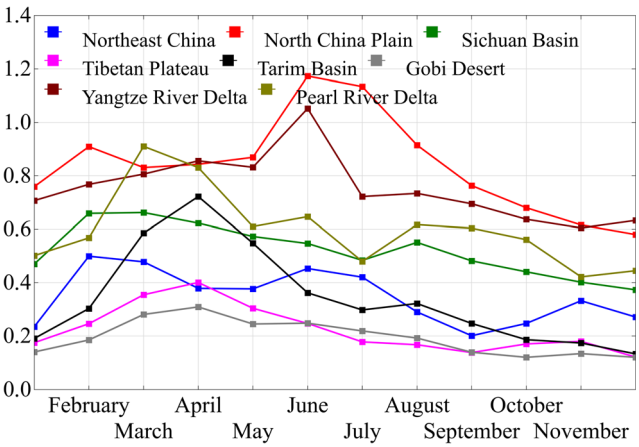

Fig. 8 Monthly AOD variations in the eight ecological regions of China during 2000–2017

factors of aerosols formation and impact. Those are Northeast China (including Liaoning, Jilin, Heilongjiang, and Eastern part of Inner Mongolia), North China Plain (including centralized municipalities in the capital region of BJ and TJ, the Central and Western parts of Hebei, Shandong, North Anhui, North-West Henan, North Jiangsu), Sichuan Basin (including Central and Eastern region of Sichuan Province and CQ city under central authority), the Tibetan Plateau, Tarim Basin, Gobi Desert (including West Xinjiang, North Gansu provinces and the Eastern part of Inner Mongolia), Yangtze River Delta (overlapping SH, the North Zhejiang and southern part of Jiangsu provinces), and the Pearl River Delta (the larger part of Guangdong Province).

High mean AOD values were observed in regions with the largest China megalopolises with high density of population and poorly controlled urban and industrial emissions, which introduce a large amount of pollutants into the atmosphere. Two typical examples are Yangtze River Delta and Pearl River Delta. Pearl River Delta has one of the fastest developing economies with fast growth of population and includes large megalopolises (Hong Kong, Guangzhou, and Shenzhen) with density of population over 1044 per km^2 (Statistics Press of China 2014). Yangtze River Delta is also characterized by fast economic growth as well as high rates of population growth. It comprises SH and other large cities of Zhejiang and Jiangsu provinces. Average population density in Yangtze River Delta is over 717 per km^2 and in SH—over 3800 per km^2 (Statistics Press of China 2014). Heavy direct emissions from city transport and industrial pollution, and secondary aerosols from the

hard photochemical and chemical reactions at high humidity and temperatures are responsible for occurrence of fine aerosol fractions in atmosphere, so-called secondary aerosols in Yangtze River Delta and Pearl River Delta, which, probably, are main sources, causing high AOD throughout a year and, consequently, high 18-year mean AOD values (0.6–0.75). They are formed not only from products of organic compounds, but also from sulfur dioxide, hydrogen sulfide, ammonia, nitrogen oxides, and some other gases with oxidizing agents like ozone as well as with water vapor and aerosol particles, playing primarily a role of catalysts.

Figure 7 presents mean AOD values over North China Plain, which give detailed illustration of urban and industrial origin of AOD over the largest megalopolises, such as BJ, TJ, SJZ, and ZZ. Heavy pollution from city transport, local biomass combustion for heating, electrical power plants, chemical and petroleum productions of companies, and associated with them secondary aerosols resulted in the higher concentration of aerosols and higher mean values of AOD (0.77–0.96).

Figure 8 details temporal variations of AOD for all listed ecological regions. For the entire study period, low aerosol levels prevailed in Gobi Desert, Tibetan Plateau, and Tarim Basin, where local naturally occurring aerosol particles dominated. In such regions as Yangtze River Delta, Pearl River Delta, North China Plain, and Sichuan Basin, where industrial particles dominate, significantly higher aerosol loadings are observed. In Gobi Desert, Tibetan Plateau, and Tarim Basin, monthly AOD values were primarily less than 0.40 during the entire study period, which may be associated with lower levels of human activity. Often dust storms in spring period, occurring predominantly over north-west and north districts of China and transporting coarse particles of dust from north to east, transfer a large amount of soil and mineral dust into air, which later in the course of transportation may significantly increase AOD in the majority of China regions and may dramatically change AOD distribution during summer. Spatial AOD variability in spring to some extent is controlled by superficial moisture content. Intensive spring heating extracts surface moisture from soil, making it dry and loose. Open, sun-dried soil is able to produce significant amounts of dust which is gradually transported into the air with the start of local wind circulation. These natural processes in Tarim Basin in the period from March to May lead to high aerosol loadings, suggesting often occurrence of dust and sandstorms in spring over the Taklamakan Desert with maximal AOD values in April 0.722.

In the period from 2000 to 2017, Yangtze River Delta, North China Plain, and Pearl River Delta with their intensive industrial activity and high density of population were, as a rule, characterized by high aerosol loadings, in the period from May to August. The reason of high AOD values in summer may be hygroscopic growth of aerosol particles in extreme humid summer seasons (Li et al. 2007; Bian et al. 2009; Che et al. 2015c; Chen et al. 2016). During the entire period, the majority of AOD values (about 80%) in these regions exceeded 0.6; this may be explained by the fact that high AOD values were observed in urban, industrial, and densely populated regions with intensive industrial activity and high density of population, which reflects the contribution of particulate matter into pollution, especially fine particles with aerodynamic diameter no more than 2.5 μm (Cheng et al. 2013), which may also be formed from combustion of agricultural crops biomass (Li et al. 2010; Xu et al. 2015).

Figure 7 also shows clear regional characteristics and significant impact of local sources of aerosols. Various seasonal AOD regularities over eight regions are shown in Fig. 8. Tarim Basin had its seasonal fluctuations with maximal aerosol loading in spring (0.586, 0.722, and 0.548 for April, March, and May, respectively) and minimal—in autumn-winter (from 0.186 in October to 0.133 in December). Seasonal AOD variations in Tibetan Plateau and Gobi Desert were similar to seasonal fluctuations in Tarim Basin, with maximal values in spring (in April 0.401 for Tibetan Plateau and 0.309 for Gobi Desert) and in summer (in June 0.247 for Tibetan Plateau and 0.248 for Gobi Desert), and minimal—in autumn-winter (from 0.120 in October to 0.185 in February for Tibetan Plateau and from 0.138 in September to 0.246 in February for Gobi Desert), suggesting reflective impact of dust events.

Similar seasonal regularities were observed in North China Plain and Yangtze River Delta with one of the highest AOD values (1.173, 1.134 0.915 and 1.052, 0.722, 0.734 for June, July, and August, respectively) in summer period, and the lowest (0.763, 0.680, 0.616 and 0.695, 0.637, 0.605 for September, October, and November, respectively) in autumn. The fact that the highest AOD values in North China Plain were in summer rather than in spring indicates that in summer photochemical interactions are more active and are followed by higher temperatures and high water vapor content in the atmosphere which increases the hygroscopic growth of fine aerosol particles (Dickerson et al. 1997). In Northeast China for the study period, minimal AOD values were observed in autumn and winter (from 0.201 in September to 0.235 in January), and maximal AOD values—in spring and summer (from 0.478 in March to 0.421 in July).

One of the main processes of both aerosol particles and gaseous impurities removal from atmosphere into soil is air purification by precipitations, which is typical for southern regions of China (Yangtze River Delta, Pearl River Delta, Tibetan Plateau, and Sichuan Basin) with beginning of monsoon rains, leading to atmosphere purification due to loaded aerosols removal through precipitations during a long-term rain season from the mid of May to September. In this season, variable local diagram of wind circulation changes to a certain regional one. Available moisture in monsoon winds combined

with sea-salt and mainland aerosols creates a vast cloud cover which causes monsoon precipitations all over South China. Therefore, aerosol particles concentration decreases during this season as they are quickly removed from the atmosphere by precipitating. Thus Pearl River Delta experienced a peak of high AOD from 0.831–0.910 in the period before the rainfall season in April and March, respectively, to 0.480 during a rainy period in July. In the course of monsoon drift to Tibetan Plateau, there was a gradual shift of precipitations northward to middle latitudes, which also caused reduction of AOD from 0.247 in June to 0.138 in September. The Yangtze River Delta territory is also exposed to summer monsoon influence. Thus, before the rainfall season, maximal values were from 0.806 to 1.052 from March to June, and the start of the rainfall season there was a reduction of AOD values up to 0.695 in September.

Some authors also presented the similar results of investigations on China, which characterized the increase of aerosol concentrations, varying from season to season, with regional natural and anthropogenic pollution (He et al. 2012a; Luo et al. 2013; Song et al. 2014; Filonchyk et al. 2018b). Also selected search algorithms (combined MODIS Dark Target and Deep Blue AOD), which uses MODIS Collection 6.1, show similar results with previous studies (Leeuw et al. 2018; Sogacheva et al. 2018). Thus, the selected algorithm, which allows to search for aerosols over dark and light patches of earth, can be used for quantitative studies of aerosols and their application in different regions.

3.5 Spatiotemporal AOD variability between cities

Data in Fig. 9 and Table 2 show considerable seasonal fluctuations of AOD values in many large cities. Trends of AOD alteration over one city follow different rules, and levels of air pollutants and trends of their alteration in different cities differ considerably. MODIS Terra aerosol product with spatial resolution 3 km was used for aerosols study within urban area. It is also seen that tendencies to AOD alteration were manifested

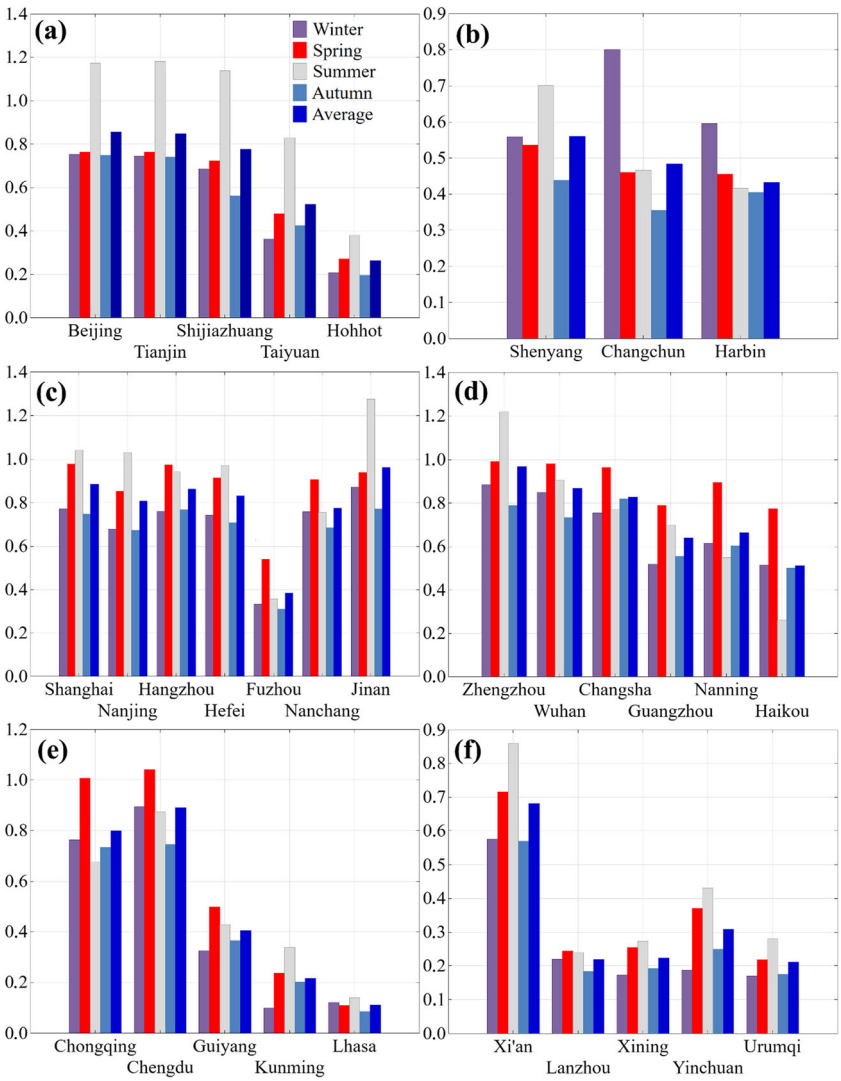

Fig. 9 Seasonal mean distribution of MODIS AOD during 2000–2017 in different geographical zones. **a** North China, **b** Northeast China, **c** East China, **d** South Central China, **e** Southwest China, **f** Northwest China

Table 2 Monthly mean distribution of MODIS AOD during 2007–2017 in 31 largest cities of China

	January	February	March	April	May	June	July	August	September	October	November	December
BJ	0.640	0.950	0.686	0.770	0.837	1.205	1.353	0.961	0.815	0.705	0.728	0.627
TJ	0.730	0.923	0.712	0.758	0.818	1.233	1.397	0.914	0.740	0.702	0.700	0.545
SJZ	0.605	1.003	0.678	0.719	0.777	1.050	1.252	1.110	0.737	0.441	0.504	0.444
TY	0.304	0.456	0.458	0.455	0.524	0.717	0.916	0.852	0.598	0.395	0.278	0.310
HH	0.195	0.241	0.284	0.245	0.285	0.359	0.420	0.361	0.279	0.180	0.130	0.178
SY	0.470	0.696	0.537	0.520	0.550	0.767	0.859	0.503	0.418	0.386	0.511	0.476
CC	0.480	1.213	0.480	0.437	0.467	0.525	0.516	0.357	0.259	0.323	0.484	0.594
HB	0.262	0.995	0.504	0.446	0.422	0.419	0.476	0.354	0.264	0.355	0.596	0.273
SH	0.763	0.863	0.905	1.026	1.007	1.254	0.948	0.929	0.770	0.711	0.760	0.697
NJ	0.705	0.747	0.845	0.857	0.860	1.327	0.891	0.876	0.760	0.681	0.577	0.586
HZ	0.712	0.863	0.954	1.000	0.975	1.148	0.838	0.846	0.812	0.775	0.718	0.714
HF	0.756	0.837	0.886	0.946	0.911	1.268	0.821	0.827	0.741	0.756	0.626	0.626
FZ	0.351	0.340	0.574	0.616	0.431	0.417	0.308	0.346	0.366	0.305	0.260	0.303
NC	0.826	0.856	0.918	0.935	0.863	0.970	0.631	0.665	0.754	0.728	0.575	0.584
JN	0.946	1.047	0.789	0.994	0.780	1.313	1.371	1.146	0.942	0.740	0.630	0.605
ZZ	0.880	1.167	0.946	1.026	1.004	1.202	1.315	1.142	0.935	0.798	0.635	0.583
WH	0.872	1.027	0.944	0.989	1.014	1.174	0.749	0.795	0.819	0.781	0.599	0.650
CS	0.877	0.787	0.810	1.041	0.907	0.822	0.635	0.598	0.910	0.912	0.636	0.602
GZ	0.512	0.599	0.866	0.906	0.594	0.845	0.600	0.722	0.666	0.580	0.423	0.448
NN	0.660	0.753	1.075	1.028	0.582	0.569	0.478	0.604	0.602	0.715	0.500	0.583
HK	0.526	0.524	0.968	0.917	0.438	0.268	0.220	0.299	0.443	0.620	0.422	0.476
CQ	0.727	1.012	1.077	1.034	0.911	0.737	0.596	0.698	0.774	0.719	0.705	0.543
CD	0.748	1.239	1.164	1.009	0.954	0.897	0.855	0.871	0.767	0.754	0.717	0.667
GY	0.381	0.299	0.526	0.495	0.477	0.481	0.397	0.410	0.393	0.356	0.347	0.293
KM	0.093	0.108	0.290	0.244	0.178	0.164	0.422	0.441	0.318	0.157	0.127	0.096
LS	0.110	0.144	0.159	0.092	0.077	0.097	0.144	0.178	0.132	0.060	0.065	0.093
XA	0.552	0.705	0.764	0.754	0.629	0.677	0.835	1.050	0.658	0.618	0.431	0.486
LZ	0.224	0.229	0.284	0.278	0.170	0.243	0.213	0.265	0.227	0.169	0.156	0.174
XN	0.116	0.218	0.242	0.280	0.241	0.275	0.272	0.276	0.232	0.197	0.146	0.128
YC	0.173	0.211	0.341	0.404	0.370	0.466	0.418	0.409	0.315	0.239	0.194	0.165
UQ	0.157	0.227	0.209	0.198	0.247	0.328	0.278	0.235	0.190	0.163	0.172	0.128
	0.308	0.395	0.494	0.494	0.411	0.424	0.366	0.349	0.294	0.279	0.260	0.242

by different regional characteristics outside city scope. Thus, 18-year mean AOD values over all China regions are characterized by high values in North (BJ 0.856, TJ 0.848), East (JN 0.963, SH 0.886, HZ 0.863), South Central (ZZ 0.969, ZH 0.868, CS 0.828), Southwest (CD 0.890, CQ 0.799), and Northwest China (XA 0.681). Minimal AOD values were only in cities of two regions: Southwest (KM 0.216, LS 0.111) and Northwest China (XN 0.223, LZ 0.219, UQ 0.211). The fact that both maximal and minimal AOD values may exist in one region (Southwest China) may suggest the importance of land forms in aerosols distribution.

Although each city has something special, they can be classified into three main types. The first is characterized by larger mean AOD values in spring and summer with the highest value in spring. One of the main reasons for high AOD in spring can be dust storms, often occurring in North China in the period from March to May (Filonchyk et al. 2018a). As seen from Fig. 8, in March and April often demonstrate peak AOD values for spring which agrees with the highest dust storms frequency (Guan et al. 2015), from which large cities of the country suffer (CD 1.042, CQ 1.007, WH 0.982, CS 0.964). Unlike the aforementioned four cities, AOD peak in spring in NC (0.906), NN (0.895), GZ (0.789), and HK (0.774) is explained by a high minor particles content and aerosol hygroscopic growth effect due to high relative humidity (Chen et al. 2014). The more precipitations fall in summer, the lower AOD is compared to spring (Deng et al. 2013).

The second type is characterized by high AOD in summer and spring with maximal values in summer. Reasons for AOD increase in summer may be conditioned by aerosol particles

Table 3 Pearson correlation coefficients between cities in the China of AOD (cells below the diagonal) and distances between cities (km) (cells above the diagonal)

	BJ	TJ	SJZ	TY	HH	SY	CC	HB	SH	NJ	HZ	HF	FZ	NC	JN	ZZ
BJ	–	108	265	402	413	627	860	1057	1068	898	1122	898	1563	1249	364	622
TJ	0.98	–	264	425	506	605	858	1068	962	800	1021	809	1468	1169	275	579
SJZ	0.9	0.88	–	172	394	866	1114	1318	988	769	1005	731	1406	1048	267	375
TY	0.86	0.82	0.89	–	336	1025	1262	1456	1099	858	1094	794	1458	1068	414	359
HH	0.84	0.82	0.9	0.96	–	987	1170	1327	1382	1163	1399	1116	1787	1403	653	697
SY	0.88	0.9	0.79	0.59	0.67	–	278	510	1188	1158	1312	1231	1790	1610	794	1157
CC	0.17	0.16	0.25	*− 0.15*	*− 0.08*	0.47	–	232	1448	1433	1578	1509	2054	1888	1067	1425
HB	0.24	0.22	0.3	*− 0.06*	*− 0.03*	0.47	0.85	–	1675	1666	1809	1742	2285	2120	1291	1642
SH	0.65	0.66	0.65	0.57	0.68	0.64	0.05	0.13	–	270	161	402	610	606	732	827
NJ	0.69	0.71	0.66	0.64	0.74	0.6	*− 0.05*	*− 0.02*	0.94	–	236	144	668	468	537	562
HZ	0.47	0.47	0.48	0.43	0.57	0.47	0.04	0.15	0.94	0.89	–	324	478	453	767	786
HF	0.55	0.58	0.53	0.46	0.59	0.53	0.06	0.09	0.94	0.96	0.95	–	674	379	535	466
FZ	*− 0.12*	*− 0.08*	0.04	0.01	0.2	*− 0.01*	*− 0.11*	*− 0.01*	0.51	0.39	0.68	0.53	–	448	1199	110
NC	0.06	0.13	0.17	0.01	0.22	0.17	0.16	0.17	0.64	0.62	0.78	0.78	0.77	–	894	706
JN	0.88	0.9	0.91	0.83	0.85	0.74	0.12	0.12	0.66	0.74	0.49	0.63	0.08	0.28	–	369
ZZ	0.84	0.85	0.94	0.82	0.88	0.74	0.23	0.3	0.71	0.72	0.61	0.67	0.25	0.43	0.92	–
WH	0.3	0.35	0.4	0.22	0.4	0.37	0.29	0.26	0.77	0.76	0.86	0.88	0.61	0.94	0.46	0.61
CS	*− 0.26*	*− 0.19*	*− 0.24*	*− 0.25*	*− 0.14*	*− 0.28*	*− 0.17*	*− 0.1*	0.2	0.18	0.4	0.36	0.61	0.74	*− 0.04*	0.08
GZ	0.26	0.28	0.38	0.41	0.53	0.2	−0.15	0.01	0.71	0.7	0.82	0.75	0.84	0.74	0.46	0.55
NN	*− 0.4*	*− 0.34*	*− 0.21*	*− 0.27*	*− 0.12*	*− 0.22*	0.07	0.18	0.1	0.02	0.33	0.2	0.84	0.61	*− 0.15*	0.02
HK	*− 0.62*	*− 0.56*	*− 0.49*	*− 0.52*	*− 0.39*	*− 0.42*	*− 0.01*	0.09	*− 0.13*	*− 0.23*	*0.12*	*− 0.03*	0.73	0.46	*− 0.44*	*− 0.27*
CQ	*− 0.19*	*− 0.16*	0.02	*− 0.18*	*− 0.02*	*− 0.02*	0.3	0.5	0.3	0.15	0.51	0.35	0.77	0.76	*− 0.05*	0.24
CD	0.2	0.21	0.42	0.15	0.3	0.39	0.58	0.71	0.44	0.32	0.57	0.46	0.6	0.66	0.27	0.55
GY	0.16	0.22	0.23	0.31	0.47	0.13	*− 0.41*	*− 0.2*	0.7	0.64	0.77	0.68	0.83	0.68	0.26	0.39
KM	0.5	0.46	0.62	0.82	0.76	0.22	*− 0.4*	*− 0.19*	0.25	0.29	0.18	0.11	0.17	*− 0.14*	0.53	0.56
LS	0.34	0.33	0.64	0.58	0.62	0.29	0.18	0.17	0.13	0.21	0.09	0.09	0.15	0.05	0.52	0.57
XA	0.52	0.49	0.75	0.8	0.78	0.3	*− 0.08*	0.05	0.43	0.46	0.38	0.36	0.3	0.16	0.66	0.75
LZ	0.19	0.22	0.45	0.38	0.5	0.18	0.01	0.06	0.48	0.5	0.52	0.5	0.71	0.58	0.52	0.55
XN	0.66	0.61	0.73	0.79	0.81	0.46	*− 0.1*	0.14	0.75	0.72	0.77	0.68	0.51	0.43	0.67	0.8
YC	0.68	0.67	0.7	0.81	0.85	0.49	*− 0.3*	*− 0.11*	0.85	0.83	0.8	0.76	0.5	0.41	0.69	0.75
UQ	0.88	0.88	0.84	0.77	0.83	0.8	0.13	0.25	0.89	0.9	0.78	0.82	0.19	0.42	0.8	0.85

	WH	CS	GZ	NN	HK	CQ	CD	GY	KM	LS	XA	LZ	XN	YC	UQ
BJ	1053	1337	1890	2046	2283	1458	1517	1731	2088	2562	911	1179	1327	891	2434
TJ	988	1277	1820	1999	2222	1442	1520	1702	2072	2603	913	1223	1380	947	2504
SJZ	828	1104	1664	1793	2041	1195	1260	1468	1824	2344	653	972	1138	721	2339
TY	825	1076	1642	1722	1994	1077	1117	1369	1703	2175	516	800	965	553	2191
HH	1163	1410	1976	2028	2315	1336	1321	1649	1942	2.233	769	864	978	531	1999
SY	1491	1784	2282	2535	2714	2036	2125	2277	2664	3189	1517	1806	1948	1502	2910
CC	1770	2062	2560	2813	2993	2299	2375	2548	2928	3399	1767	2019	2147	1699	2999
HB	1999	2292	2792	3040	322	2510	2574	2767	3140	3560	1968	2188	2304	1859	3060

Table 3 (continued)

SH	689	885	1212	1600	1667	1440	1658	1523	1959	2904	1217	1714	1910	1600	3268
NJ	459	704	1133	1455	1578	1199	1404	1317	1750	2646	947	1444	1640	1.338	3008
HZ	566	735	1052	1440	1507	1313	1542	1377	1812	2790	1142	1646	1843	1563	3228
HF	320	581	1050	1339	1485	1056	1262	1180	1611	2505	821	1323	1518	1240	2904
FZ	704	670	694	1169	1134	1312	1575	1255	1667	2792	1349	1841	2034	1841	3466
NC	261	287	671	997	1110	908	1159	929	1364	2398	902	1393	1585	1402	3017
JN	722	1014	1549	1752	1958	1252	1368	1483	1875	2522	776	1179	1358	965	2603
ZZ	467	732	1295	1425	1668	882	1004	1124	1507	2188	434	900	1093	776	2444
WH	–	293	836	1046	1236	750	976	860	1291	2224	646	1143	1337	1141	2763
CS	0.58	–	565	759	945	643	904	643	1077	2129	775	1225	1407	1299	2847
GZ	0.68	0.46	–	506	455	979	1238	763	1090	2316	1309	1700	1862	1831	3284
NN	0.38	0.54	0.65	–	372	770	969	449	620	1873	1274	1534	1660	1751	3008
HK	0.18	0.56	0.43	0.94	–	1125	1338	815	959	2209	1587	1890	2024	2086	3380
CQ	0.63	0.61	0.6	0.81	0.72	–	268	331	629	1490	569	765	903	990	2305
CD	0.67	0.27	0.58	0.63	0.44	0.86	–	522	639	1248	606	599	696	890	2056
GY	0.58	0.46	0.81	0.49	0.37	0.53	0.39	–	435	1565	880	1088	1211	1322	2573
KM	*− 0.09*	*− 0.21*	0.44	0.01	*− 0.16*	*− 0.05*	0.11	0.38	–	1253	1188	1230	1292	1530	2496
LS	0.12	*− 0.32*	0.36	0.18	*− 0.06*	0.17	0.46	0.13	0.67	–	1754	1382	1255	1701	1604
XA	0.27	*− 0.1*	0.6	0.21	*− 0.07*	0.19	0.44	0.39	0.83	0.76	–	504	701	524	2118
LZ	0.51	0.23	0.85	0.65	0.4	0.53	0.58	0.58	0.49	0.7	0.69	–	197	343	1626
XN	0.54	0.2	0.79	0.23	*− 0.02*	0.37	0.52	0.64	0.7	0.42	0.79	0.59	–	447	1440
YC	0.52	0.15	0.76	0.09	*− 0.14*	0.19	0.31	0.76	0.68	0.31	0.7	0.54	0.93	–	1668
UQ	0.64	*− 0.02*	0.52	*− 0.17*	*− 0.42*	0.13	0.42	0.5	0.4	0.3	0.52	0.34	0.77	0.82	–

The negative correlation values are given in italics

growth in humid summer climate and formation of secondary fine particles by conversion of gases into particles, rising in summer due to higher solar fluxes (Xin et al. 2007; He et al. 2012a). Summer events may additionally contribute to high AOD values over East China (Lee et al. 2006). Although a great amount of precipitations decreases aerosols amount, an essential source of AOD formation in summer is also a high speed of photochemical reactions coupled with anthropogenic emissions (He et al. 2016), which contribute to AOD accumulation in the atmosphere of large cities of North (TJ 1.181, BJ 1.173, SJZ 1.138, TY 0.829), East (JN 1.276, SH 1.044, NJ 1.031, HF 0.972), and South Central China (ZZ 1.220). The similar seasonal peculiarity was observed in SY (0.701), this is proved by the result received based on sun photometer measurement (Zhao et al. 2013).

The third type is characterized by high AOD in winter period. One of the reasons for that is that winter is a by-product of the heating season in North China, especially in Northeast China (CC 0.801 and HB 0.596). For these cities, the particulate matter concentrations in winter are about 1.4–1.6 times higher, than in other seasons (Hong et al. 2010; Huang et al. 2010). Thus, February is the most polluted month with AOD values in these cities, 1.213 and 0.995 for CC and HB, respectively. Meanwhile, gradual increase of snow-ice cover on the ground prevents soil erosion and, thus, restricts emission of coarse mineral particles into the atmosphere, this suggests that principal atmosphere pollutants are secondary aerosols, which are formed in the course of fossil fuel burning. More precipitations and absent of heating in summer and autumn contribute to less pollution.

Also to study regional correlation of air pollution between different cities of the country, Pearson's correlation analysis was carried out. Table 3 presents correlation ratios (r) of daily mean AOD values between all large cities in the country. The majority of cities pairs showed positive correlation, suggesting existence of relationship between cities, which denotes similar sources of aerosols formation, such as secondary organic aerosol (SOA) or organic dust, which usually has broader regional distributions, than anthropogenic pollutants. Cities pairs, located in one geographical region of China and at nearer distance from one another, showed higher correlations, suggesting clear regional dependence in aerosols distribution. CS, NN, HK, and CQ in South Central China, FZ and NJ in East China as well as KM, GY, and LS in Southwest China correlated poorly, than other cities. These cities were predominantly exposed to local sources of pollution, which corresponds to results, obtained by Hu et al. (2014).

In this study, correlation ratios were additionally compared, taking into account distance between all cities under review. Distance between cities and results of correlation are presented in Table 3 and in Fig. 10. Strong dependence were found between r values and distance between cities. When distance

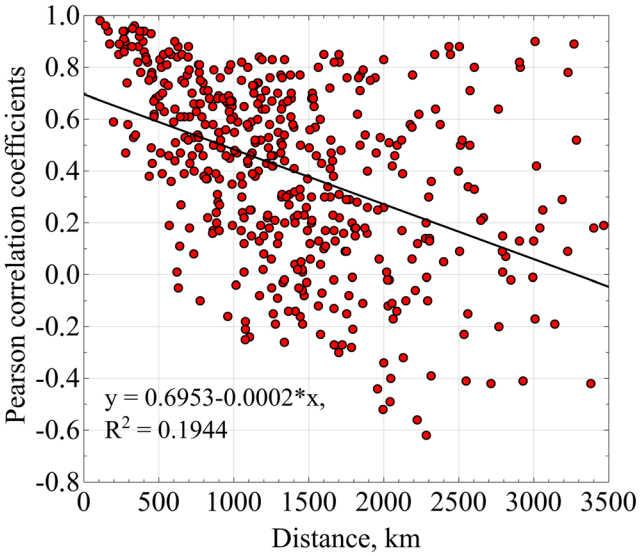

Fig. 10 Pearson correlation coefficients of AOD between cities in China

between cities were over 1500 km, Pearson correlation coefficient for AOD, exceeding 0.6, occurred rarely. As distance between cities increased, correlation values decreased, and negative values are highlighted in bold in table. However, this regularity is not applicable to UQ, demonstrating high values of ratio between distance and r value, suggesting similar mechanisms (processes) of aerosols variability and formation (Sakerin et al. 2012).

These results suggest that any city districts need coordinated regional controls in addition to local emissions control. It is obvious that the reasons for intermonth variability of aerosol thickening in various cities are uniformity of annual AOD variation nature and impact of total atmosphere circulation. It is advisable to provide a relevant analysis of AOD relationship with various indexes of atmospheric circulation in future studies.

4 Conclusion

Spatial and temporal distribution of multi-year annual, seasonal, monthly average AOD at 550 nm over various China regions was analyzed with Terra satellite-based Level 2/3 MODIS combined Dark Target and Deep Blue product for the period 2000–2017. Results of the ongoing study are the following:

1. Annual average temporal series of AOD over the entire territory of the country showed a trend to decline from 0.392 in 2000 to 0.267 in 2017 with gradual decrease by 0.125. In spring, reduction from 0.420 in 2000 to 0.331 in 2017 with decrease by 0.089 occurs in the trend of AOD alteration. Summer AOD values demonstrate sinusoidal

form with distinct peaks in 2003 (0.449), 2007 (0.424), 2011 (0.451), and 2014 (0.416) with gradual reduction of values from 0.449 in 2007 to 0.292 in 2017 with decrease of value by 0.125. In general, a trend to gradual decrease of AOD values was observed over the entire territory of the country.

2. It was found that maximal annual mean AOD values (over 0.7) occur in eastern parts of the country (such as Yangtze River Delta, North China Plain, Pearl River Delta) as well as Sichuan Basin, and minimal ones (up to 0.25)—in sparsely populated areas on the Tibetan plateau and in the north forest ecosystems in the north-eastern part of China.
3. High AOD values over China regions may be explained by rapid rates of urbanization, characterized by anthropogenic aerosols emissions as a result of increase of truck transportation, industrial emissions, a large amount of construction works as well as increase the amount of aerosols, formed in result of biomass combustion. High density of population, relief, climate, and economics are also closely related to aerosol climatology over China.
4. There are three types of seasonal AOD alteration: the first type shows higher AOD in spring and summer with monthly AOD peak, manifesting in spring (CD 1.042, CQ 1.007, WH 0.982, CS 0.964, NC 0.906, NN 0.895, GZ 0.789, HK 0.774). The second type shows maximal monthly AOD in summer (TJ 1.181, BJ 1.173, SJZ 1.138, TY 0.829, JN 1.276, SH 1.044, NJ 1.031, HF 0.972, ZZ 1.220, SY 0.701) and the second largest in spring. The third type shows maximal monthly AOD in winter (CC 0.801, HB 0.596).
5. Eighteen years mean AOD values over all China regions are characterized by high values in North (BJ 0.856, TJ 0.848), East (JN 0.963, SH 0.886, HZ 0.863), South (ZZ 0.969, ZH 0.868, CS 0.828), Southwest (CD 0.890, CQ 0.799), and Northwest China (XA 0.681). Minimal AOD values were only in cities of two regions: Southwest (KM 0.216, LS 0.111) and Northwest China (XN 0.223, LZ 0.219, UQ 0.211).
6. Spatial variations in Ångström exponent distribution over China demonstrate a range from 0.31 to 1.7 for the most part of the country, lower values between 0.31 and 0.84 were in the north and north-west of the country, and the higher values—in the south (1.3–1.7). One of the main sources of coarse particles formation as a result of wind erosion is the Taklamakan Desert. There is a tendency towards increase of AOD with decrease of Ångström exponent, which means the presence of coarse particles in atmosphere.
7. In general, there is a gradual decrease in the aerosol load on the territory of the country. The main reason of improving the air quality of the territory is a clear directional policy of the government to improve the environmental safety of the country, which is not only aimed at improving air quality, but also improving the overall environmental situation on the territory.

Although this study addressed the study of aerosols properties in many regions of China that can not only promote better assessment of air quality, weather, and climate change, but also to make a significant contribution to research in the field of environment, epidemiology, and health as well as to make recommendations on elaboration of state policy in the field of environmental protection. However, to obtain more reliable information on aerosols, it is necessary to use not only satellite data, but also ground-based sun-photometric measurements, which are based on CSHNET (Chinese Sun Hazemeter Network) and AERONET stations. This gives more accurate information due to the very low measurement error. Further on, it is necessary to conduct additional studies, aimed at research of AOD and Ångström exponent relationship as well as their impact on cloud parameters such as water vapor, cloud effective radius, cloud optical thickness, cloud top temperature, cloud fraction, and cloud top pressure. As well as use of complex approach in AOD climatology research with use of data from various instruments, including both ground-based and satellite data.

Acknowledgements The authors would like to express our gratitude to the Atmosphere Archive and Distribution System (LAADS) and NASA's Giovanni web site for providing the MODIS AOD products.

Funding information The work was financially supported by the China Postdoctoral Science Foundation Funded Project (2018M633605), the Postdoctoral Fund of Lanzhou Jiaotong University (2018BH03001), and the National Key R&D Program of China (2017YFB0504203 and 2017YFB0504201).

References

Bian H, Chin M, Rodriguez JM, Yu H, Penner JE, Strahan S (2009) Sensitivity of aerosol optical thickness and aerosol direct radiative effect to relative humidity. Atmos Chem Phys 9:2375–2386

Bilal M, Nichol JE (2015) Evaluation of MODIS aerosol retrieval algorithms over the Beijing-Tianjin-Hebei region during low to very high pollution events. J Geophys Res Atmos 120(15):7941–7957

Che H, Wang Y, Sun J, Zhang X, Zhang X, Guo J (2013) Variation of aerosol optical properties over the Taklimakan Desert in China. Aerosol Air Qual Res 13:777–785

Che H, Xia X, Zhu J, Wang H, Wang Y, Sun J, Shi G (2015a) Aerosol optical properties under the condition of heavy haze over an urban site of Beijing, China. Environ Sci Pollut Res 22(2):1043–1053

Che H, Zhang XY, Xia X, Goloub P, Holben B, Zhao H, Wang Y, Zhang XC, Wang H, Blarel L (2015b) Ground-based aerosol climatology of China: aerosol optical depths from the China aerosol remote sensing network (CARSNET) 2002–2013. Atmos Chem Phys 15: 7619–7652

Che H, Zhao H, Wu Y, Xia X, Zhu J, Wang H, Wang Y, Sun J, Yu J, Zhang X (2015c) Analyses of aerosol optical properties and direct radiative forcing over urban and industrial regions in northeast China. Meteorog Atmos Phys 127:345–354

Chen J, Xin J, An J, Wang Y, Liu Z, Chao N, Meng Z (2014) Observation of aerosol optical properties and particulate pollution at background station in the Pearl River Delta region. Atmos Res 143:216–227

Chen W, Tang H, Zhao H, Yan L (2016) Analysis of aerosol properties in Beijing based on ground-based sun photometer and air quality monitoring observations from 2005 to 2014. Remote Sens 8(2):110

Cheng Z, Wang S, Jiang J, Fu Q, Chen C, Xu B, Hao J (2013) Long-term trend of haze pollution and impact of particulate matter in the Yangtze River Delta, China. Environ Pollut 182:101–110

Cui Q, Pan D, Bai Y, He X, Chen J (2012) Assessment of suspended particulate matter concentration retrieved by Aqua-MODIS and SeaWiFS in the East China Sea, Proc. SPIE, Remote Sensing of the Ocean, Sea Ice, Coastal Waters, and Large Water Regions 2012, (October 19, 2012), pp. 85320Y-85327

Deng X, Wu D, Yu J, Lau AKH, Li F, Tan H, Yuan Z, Ng WM, Deng T, Wu C, Zhou X (2013) Characterization of secondary aerosol and its extinction effects on visibility over the Pearl River Delta Region, China. J Air Waste Manag Assoc 63:1012–1021

Dickerson R, Kondragunta S, Stenchikov G, Civerolo K, Doddridge B, Holben B (1997) The impact of aerosols on solar ultraviolet radiation and photochemical smog. Science 278:827–830

Filonchyk M, Yan H, Yang S, Hurynovich V (2016) A study of PM2.5 and PM10 concentrations in the atmosphere of large cities in Gansu Province, China, in summer period. J Earth Syst Sci 125(6):1175–1187

Filonchyk M, Yan H, Yang S, Lu X (2018a) Detection of aerosol pollution sources during sandstorms in Northwestern China using remote sensed and model simulated data. Adv Space Res 61(4):1035–1046

Filonchyk M, Yan H, Shareef TME, Yang S (2018b) Aerosol contamination survey during dust storm process in Northwestern China using ground, satellite observations and atmospheric modeling data. Theor Appl Climatol:1–15. https://doi.org/10.1007/s00704-017-2362-8

Ge JM, Huang JP, Xu CP, Qi YL, Liu HY (2015) Characteristics of Taklamakan dust emission and distribution: a satellite and reanalysis field perspective. J Geophys Res Atmos 119(20):772–783

Georgeson L, Maslin M, Poessinouw M, Howard S (2016) Adaptation responses to climate change differ between global megacities. Nat Clim Chang 6(6):584–588

Gerelmaa D, Liu GR, Kuo TH, Lin TH (2016) Investigation of permanent aerosol source regions over Asia using multi-year MODIS observations. J Mar Sci Tech 24(2):269–281

Guan Q, Yang J, Zhao S, Pan B, Liu C, Zhang D, Wu T (2015) Climatological analysis of dust storms in the area surrounding the Tengger Desert during 1960–2007. Clim Dyn 45(3–4):903–913

He Q, Li C, Tang X, Li H, Geng F, Wu Y (2010) Validation of MODIS derived aerosol optical depth over the Yangtze River Delta in China. Remote Sens Environ 114(8):1649–1661

He Q, Li C, Geng F, Lei G, Li Y (2012a) Study on long-term aerosol distribution over the land of East China using MODIS data. Aerosol Air Qual Res 12:304–319

He Q, Li C, Geng F, Yang H, Li P, Li T, Liu D, Pei Z (2012b) Aerosol optical properties retrieved from sun photometer measurements over Shanghai, China. J Geophys Res 117:D16204. https://doi.org/10.1029/2011JD017220

He Q, Zhou G, Geng F, Gao W, Yu W (2016) Spatial distribution of aerosol hygroscopicity and its effect on PM2.5 retrieval in East China. Atmos Res 170:161–167

Holben BN, Eck TF, Slutsker I, Tanre D, Buis JP, Setzer A, Lavenu F (1998) AERONET—a federated instrument network and data archive for aerosol characterization. Remote Sen Environ 66(1):1–16

Hong Y, Zhou D, Qi Y, Liu D, Ma Y, Liu N, Gan L (2010) Distribution characteristics of aerosol mass concentrations in northeastern China. Arid Land Geogr 33:224–230 (in Chinese)

Hsu NC, Tsay SC, King MD, Herman JR (2004) Aerosol properties over bright-reflecting source regions. IEEE Trans Geosci Remote Sen 42(3):557–569

Hsu NC, Tsay SC, King MD, Herman JR (2006) Deep blue retrievals of Asian aerosol properties during ACE-Asia. IEEE Trans Geosci Remote Sen 44(11):3180–3195

Hsu NC, Jeong MJ, Bettenhausen C, Sayer AM, Hansell R, Seftor CS, Huang J, Tsay SC (2013) Enhanced deep blue aerosol retrieval algorithm: the second generation. J Geophys Res Atmos 118:9296–9315

Hu J, Wang Y, Ying Q, Zhang H (2014) Spatial and temporal variability of PM2.5 and PM10 over the North China Plain and the Yangtze River Delta, China. Atmos Environ 95:598–609

Huang L, Wang K, Yuan C-S, Wang G (2010) Study on the seasonal variation and source apportionment of PM10 in Harbin, China. Aerosol Air Qual Res 10:86–93

Huang J, Ji M, Xie Y, Wang S, He Y, Ran J (2016) Global semi-arid climate change over last 60 years. Clim Dyn 46:1131–1150

Huang Y, Yan Q, Zhang C (2018) Spatial–temporal distribution characteristics of PM 2.5 in China in 2016. J Geovis Spat Anal 2(2):12

Ichoku C, Chu DA, Mattoo S, Kaufman YJ, Remer LA, Tanré D, Holben BN, (2002) A spatio-temporal approach for global validation and analysis of MODIS aerosol products. Geophys Res Lett 29(12):1616. https://doi.org/10.1029/2001GL013206

Kang N, Kumar KR, Yin Y, Diao Y, Yu X (2015) Correlation analysis between AOD and cloud parameters to study their relationship over China using MODIS data (2003–2013): impact on cloud formation and climate change. Aerosol Air Qual Res 15:958–973

Kang N, Kumar KR, Hu K, Yu X, Yin Y (2016) Long-term (2002–2014) evolution and trend in collection 5.1 level-2 aerosol products derived from the MODIS and MISR sensors over the Chinese Yangtze River Delta. Atmos Res 181:29–43

Kaufman YJ, Tanré D, Remer LA, Vermote EF, Chu A, Holben BN (1997) Operational remote sensing of tropospheric aerosol over land from EOS moderate resolution imaging spectroradiometer. J Geophys Res Atmos 102(27):51–17

Kaufman YJ, Koren I, Remer LA, Rosenfeld D, Rudich Y (2005) The effect of smoke, dust, and pollution aerosol on shallow cloud development over the Atlantic Ocean. Proc Natl Acad Sci 102:11207–11212

Kim DH, Sohn BJ, Nakajima T, Takamura T, Takemura T, Choi BC, Yoon SC (2004) Aerosol optical properties over East Asia determined from ground-based sky radiation measurements. J Geophys Res Atmos 109(D2):D02209. https://doi.org/10.1029/2003JD003387

Lee KH, Kim YJ, Kim MJ (2006) Characteristics of aerosol observed during two severe haze events over Korea in June and October 2004. Atmos Environ 40:5146–5155

Lee HJ, Chatfield RB, Strawa AW (2016) Enhancing the applicability of satellite remote sensing for PM2.5 estimation using MODIS deep blue AOD and land use regression in California, United States. Environ Sci Technol 50(12):6546–6555

Leeuw GD, Sogacheva L, Rodriguez E, Kourtidis K, Georgoulias AK, Alexandri G (2018) Two decades of satellite observations of AOD over mainland China using ATSR-2, AATSR and MODIS/Terra: data set evaluation and large-scale patterns. Atmos Chem Phys 18(3):1573–1592

Levy RC, Remer LA, Mattoo S, Vermote EF, Kaufman YJ (2007) Second-generation operational algorithm: retrieval of aerosol properties over land from inversion of Moderate Resolution Imaging Spectroradiometer spectral reflectance. J Geophys Res Atmos 112(D13)

Levy RC, Remer LA, Kleidman RG, Mattoo S, Ichoku C, Kahn R, Eck TF (2010) Global evaluation of the Collection 5 MODIS dark-target aerosol products over land. Atmos Chem Phys 10(21):10399–10420

Levy RC, Mattoo S, Munchak LA, Remer LA, Sayer AM, Patadia F, Hsu NC (2013) The Collection 6 MODIS aerosol products over land and ocean. Atmos Meas Tech 6(11):2989–3034

Li Z, Niu F, Lee KH, Xin J, Hao WM, Nordren B, Wang Y, Wang P (2007) Validation and understanding of Moderate Resolution Imaging Spectroradiometer aerosol products (C5) using ground-based measurements from the handheld sun photometer network in China. J Geophys Res Atmos 112:D22S07. https://doi.org/10.1029/2007JD008479

Li B, Yuan H, Niu F, Tao S (2010) Spatial and temporal variations of aerosol optical depth in China during the period from 2003 to 2006. Int J Remote Sens 31:1801–1817

Li Z, Zhao S, Edwards R, Wang W, Zhou P (2011) Characteristics of individual aerosol particles over Ürümqi Glacier No. 1 in eastern Tianshan, central Asia, China. Atmos Res 99(1):57–66

Li X, Xia X, Wang S, Mao J, Liu Y (2012) Validation of MODIS and Deep Blue aerosol optical depth retrievals in an arid/semi-arid region of northwest China. Particuology 10(1):132–139

Luo Y, Daren L, Xiuji Z, Weiliang L, Qing H (2001) Characteristics of the spatial distribution and yearly variation of aerosol optical depth over China in last 30 years. J Geophys Res Atmos 106:14501–14513

Luo Y, Zheng X, Zhao T, Chen J (2013) A climatology of aerosol optical depth over China from recent 10 years of MODIS remote sensing data. Int J Climatol 34:863–870

Penner JE, Andreae MO, Annegarn H, Barrie L, Feichter J, Hegg D, Pitari G (2001) Aerosols, their direct and indirect effects. In: Climate change 2001: the scientific basis. Contribution of Working Group I to the Third Assessment Report of the Intergovernmental Panel on Climate Change. Cambridge University Press, Cambridge, pp 289–348

Platnick S, King MD, Ackerman SA, Menzel WP, Baum BA, Riédi JC, Frey RA (2003) The MODIS cloud products: algorithms and examples from Terra. IEEE Trans Geosci Remote Sens 41:459–473

Platnick S, Meyer KG, King MD, Wind G, Amarasinghe N, Marchant B, Yang P (2017) The MODIS cloud optical and microphysical products: Collection 6 updates and examples from Terra and Aqua. IEEE Trans Geosci Remote Sens 55:502–525

Qi YL, Ge JM, Huang JP (2013) Spatial and temporal distribution of MODIS and MISR aerosol optical depth over northern China and comparison with AERONET. Chin Sci Bull 58(20):2497–2506

Qiu X, Duan L, Gao J, Wang S, Chai F, Hu J, Yun Y (2016) Chemical composition and source apportionment of PM10 and PM2.5 in different functional areas of Lanzhou, China. J Environ Sci 40:75–83

Remer LA, Kaufman YJ, Tanré D, Mattoo S, Chu DA, Martins JV (2005) The MODIS aerosol algorithm, products, and validation. J Atmos Sci 62(4):947–973

Sakerin SM, Andreev SY, Bedareva TV, Kabanov DM, Poddubnyi VA, Luzhetskaya AP (2012) Spatiotemporal variations in the atmospheric aerosol optical depth on the territory of Povolzhye, Urals, and Western Siberia. Opt Atmos Okeana 25(11):958–962

Sayer AM, Munchak LA, Hsu NC, Levy RC, Bettenhausen C, Jeong MJ (2014) MODIS Collection 6 aerosol products: comparison between Aqua's e-Deep Blue, Dark Target, and "merged" data sets, and usage recommendations. J Geophys Res Atmos 119(24):13,965–13,989

Sayer AM, Hsu NC, Bettenhausen C, Jeong MJ, Meister G (2015) Effect of MODIS Terra radiometric calibration improvements on Collection 6 Deep Blue aerosol products: validation and Terra/Aqua consistency. Geophys Res Atmos 120(23):12157–12174

Seinfeld JH, Pandis SN (1998) Atmospheric chemistry and physics: from air pollution to climate change. John Wiley, New York

Sellers WD (1969) A global climatic model based on the energy balance of the earth-atmosphere system. J Appl Meteorol 8(3):392–400

Shi Y, Zhang J, Reid JS, Hyer EJ, Eck TF, Holben BN, Kahn RA (2011) Where do we need additional in situ aerosol and sun photometer data: a critical examination of spatial biases between MODIS and MISR aerosol products. Atmos Meas Tech Discuss 4:4295–4323

Sogacheva L, Leeuw GD, Rodriguez E, Kolmonen P, Georgoulias AK, Alexandri G, Xue Y (2018) Spatial and seasonal variations of aerosols over China from two decades of multi-satellite observations–part 1: ATSR (1995–2011) and MODIS C6.1 (2000–2017). Atmos Chem Phys 18(15):11389–11407

Song W, Jia H, Huang J, Zhang Y (2014) A satellite-based geographically weighted regression model for regional PM2.5 estimation over the Pearl River Delta region in China. Remote Sens Environ 154(1–7):1–7

Statistics Press of China (2014) Population yearbook of China: 2014. Statistics Press of China, Beijing

Thurston GD, Jiyoung A, Cromar KR, Shao Y, Reynolds HR, Michael J, Lim CC, Ryan S, Yikyung P, Hayes RB (2015) Ambient particulate matter air pollution exposure and mortality in the NIH-AARP diet and health cohort. Environ Health Perspect 124:484–490

Wang Y, Zhang W, Kong L, Wang J (2013) Analysis of applicability and characteristics of MODIS aerosol products in agricultural regions. Remot Sens Technol Appl 28(3):505–510 (in Chinese)

Watts N, Adger WN, Agnolucci P, Blackstock J, Byass P, Cai W, Chaytor S, Colbourn T, Collins M, Cooper A, Cox PM, Depledge J, Drummond P, Ekins P, Galaz V, Grace D, Graham H, Grubb M, Haines A, Hamilton I, Hunter A, Jiang X, Li M, Kelman I, Liang L, Lott M, Lowe R, Luo Y, Mace G, Maslin M, Nilsson M, Oreszczyn T, Pye S, Quinn T, Svensdotter M, Venevsky S, Warner K, Xu B, Yang J, Yin Y, Yu C, Zhang Q, Gong P, Montgomery H, Costello A (2015) Health and climate change: policy responses to protect public health. Lancet 386(10006):1861–1914

Xia X, Chen H, Goloub P, Zhang W, Chatenet B, Wang P (2007) A compilation of aerosol optical properties and calculation of direct radiative forcing over an urban region in northern China. J Geophys Res Atmos 112(D12)

Xia X, Wang P, Wang Y, Li Z, Xin J, Liu J, Chen H (2008) Aerosol optical depth over the Tibetan Plateau and its relation to aerosols over the Taklimakan Desert. Geophys Res Lett 35(16)

Xia X, Chen H, Goloub P, Zong X, Zhang W, Wang P (2013) Climatological aspects of aerosol optical properties in North China Plain based on ground and satellite remote-sensing data. J Quant Spectrosc Radiat Transf 127:12–23

Xin J, Wang Y, Li Z, Wang P, Hao WM, Nordgren BL, Sun Y (2007) Aerosol optical depth (AOD) and Ångström exponent of aerosols observed by the Chinese Sun Hazemeter Network from August 2004 to September 2005. J Geophys Res Atmos 112:D05203. https://doi.org/10.1029/2006JD007075

Xin J, Zhang Q, Wang L, Gong C, Wang Y, Liu Z, Gao W (2014) The empirical relationship between the PM2.5 concentration and aerosol optical depth over the background of North China from 2009 to 2011. Atmos Res 138:179–188

Xu S, Liu W, Tao S (2006) Emission of polycyclic aromatic hydrocarbons in China. Environ Sci Technol 40(3):702–708

Xu X, Qiu J, Xia X, Sun L, Min M (2015) Characteristics of atmospheric aerosol optical depth variation in China during 1993–2012. Atmos Environ 119:82–94

Ye X, She B, Benya S (2018) Exploring regionalization in the network urban. J Geovis Spat Anal 2(1):4

You W, Zang Z, Pan X, Zhang L, Chen D (2015) Estimating PM2.5 in Xi'an, China using aerosol optical depth: a comparison between the MODIS and MISR retrieval models. Sci Total Environ 505:1156–1165

Zhang J, Reid JS (2010) A decadal regional and global trend analysis of the aerosol optical depth using a data-assimilation grade over-water MODIS and Level 2 MISR aerosol products. Atmos Chem Phys 10(22):10949–10963

Zhao H, Che H, Zhang X, Ma Y, Wang Y, Wang X, Liu C, Hou B, Che H (2013) Aerosol optical properties over urban and industrial region of northeast China by using ground-based sun-photometer measurement. Atmos Environ 75:270–278

Zong X, Xia X, Che H (2015) Validation of aerosol optical depth and climatology of aerosol vertical distribution in the Taklimakan Desert. Atmos Pollut Res 6(2):239–244